nature metabolism

ARTICLES

https://doi.org/10.1038/s42255-018-0009-4

Slc12a8 is a nicotinamide mononucleotide transporter

Alessia Grozio[1], Kathryn F. Mills[1], Jun Yoshino[2], Santina Bruzzone[3], Giovanna Sociali[3], Kyohei Tokizane[1], Hanyue Cecilia Lei[1], Richard Cunningham[4], Yo Sasaki[5], Marie E. Migaud[4] and Shin-ichiro Imai[1]*

Nicotinamide mononucleotide (NMN) is a biosynthetic precursor of nicotinamide adenine dinucleotide (NAD^+) known to promote cellular NAD^+ production and counteract age-associated pathologies associated with a decline in tissue NAD^+ levels. How NMN is taken up into cells has not been entirely clear. Here we show that the *Slc12a8* gene encodes a specific NMN transporter. We find that *Slc12a8* is highly expressed and regulated by NAD^+ in the mouse small intestine. *Slc12a8* knockdown abrogates the uptake of NMN in vitro and in vivo. We further show that Slc12a8 specifically transports NMN, but not nicotinamide riboside, and that NMN transport depends on the presence of sodium ion. *Slc12a8* deficiency significantly decreases NAD^+ levels in the jejunum and ileum, which is associated with reduced NMN uptake as traced by doubly labelled isotopic NMN. Finally, we observe that *Slc12a8* expression is upregulated in the aged mouse ileum, which contributes to the maintenance of ileal NAD^+ levels. Our work identifies a specific NMN transporter and demonstrates that Slc12a8 has a critical role in regulating intestinal NAD^+ metabolism.

It has been well documented that NAD^+ declines during ageing in many tissues—including skeletal muscle, liver, adipose tissue, brain, pancreas, spleen, heart, kidney and lung—contributing to the development of various age-associated pathophysiologies[1–4]. This phenomenon is caused, at least in part, by two molecular events: the age-associated decrease in NAD^+ biosynthesis mediated by nicotinamide phosphoribosyltransferase (NAMPT), which is the rate-limiting NAD^+ biosynthetic enzyme in mammals[5], and the age-associated increase in NAD^+ consumption mediated by NAD^+-consuming enzymes, such as poly(ADP ribose) polymerases[6] and CD38 (ref. [7]). In mammalian NAD^+ biosynthesis, nicotinamide is a predominant precursor, and NAMPT catalyses the conversion of nicotinamide and 5′-phosphoribose pyrophosphate into nicotinamide mononucleotide (NMN), a key NAD^+ intermediate[8,9]. NMN is also synthesized from nicotinamide riboside (NR), another NAD^+ intermediate, by the NR kinases, NRK1 and NRK2 (ref. [10]). NMN, together with ATP, is then converted into NAD^+ by NMN adenylyltransferases, NMNAT1–3. A number of studies have reported that NMN conveys remarkable effects of improving disease conditions and mitigating age-associated physiological decline[5,11–18]. For example, NMN treatment is able to restore glucose-stimulated insulin secretion in aged C57BL/6 mice, and some genetic mouse models that show reduced insulin-secreting capability[19,20]. NMN also enhances insulin sensitivity and secretion in mouse models of diet- and age-induced type 2 diabetes or obesity[5,11]. NMN has also been shown to prevent ischaemia–reperfusion injury in the heart[18]. In addition, NMN maintains the neural stem/progenitor cell population in the aged hippocampus, improves mitochondrial function in aged skeletal muscle and reverses arterial dysfunction in aged mice[12,13,16]. In rodent models of Alzheimer's disease, NMN is able to protect mitochondrial and cognitive functions[14,17]. We have also demonstrated previously that NMN effectively mitigates age-associated physiological decline in regular chow–fed wild-type mice[15]. Collectively, these findings strongly suggest that NMN is a critical endogenous compound for NAD^+ biosynthesis and can be used as an efficient therapeutic and in preventive intervention against many age-associated disease conditions.

We have previously shown that NMN is absorbed from the gut into blood circulation within 2–3 min and transported into tissues within 10–30 min (refs [5,15]). NMN is then immediately utilized for NAD^+ biosynthesis, significantly increasing NAD^+ content in tissues over 60 min. This fast pharmacokinetics has recently been confirmed by using doubly labelled isotopic NMN (C13-D-NMN), showing its rapid absorption and conversion to NAD^+ in peripheral tissues[15]. It has also been proposed that NMN is converted extracellularly to NR, which is transported into cells and reconverted to NMN[21]. Recent studies, however, have shown that the analyses of in vivo kinetics of these NAD^+ intermediates are affected by differences in sample collection and extraction methodologies[22,23] (also see Methods). Therefore, it is critical to understand the mechanism by which NMN or NR is transported into cells or tissues. The fast pharmacokinetics of NMN led us to the hypothesis that there is an effective transporter that facilitates the direct uptake of NMN into the gut and other organs. Thus, we set out to identify this presumed NMN transporter in mammals.

Results

Identification of an NMN transporter. In our previous studies, we noticed that when NAMPT-mediated NAD^+ biosynthesis was inhibited by FK866, a potent NAMPT inhibitor, in various types of primary cells, co-administration of NMN always produced higher NAD^+ increases compared with those that NMN induces in the absence of FK866 (refs [5,16,20]). Thus, we hypothesized that the expression of a presumed NMN transporter might be upregulated when NAD^+ levels decrease. On the basis of this hypothesis, we conducted gene expression profiling in FK866-treated primary mouse

[1]Department of Developmental Biology, Washington University School of Medicine, St. Louis, MO, USA. [2]Center for Human Nutrition, Division of Geriatrics and Nutritional Science, Department of Medicine, Washington University School of Medicine, St. Louis, MO, USA. [3]Department of Experimental Medicine, Section of Biochemistry, and Center of Excellence for Biomedical Research, University of Genova, Genova, Italy. [4]Mitchell Cancer Institute, University of South Alabama, Mobile, AL, USA. [5]Department of Genetics, Washington University School of Medicine, St. Louis, MO, USA. *e-mail: imaishin@wustl.edu

hepatocytes, pancreatic islets and hippocampal neurospheres, searching for genes commonly upregulated in these three primary cultures. We focused our searches to genes that encode transporters or transmembrane proteins and found only one gene that met these criteria but whose function was unknown. This gene, *Slc12a8*, exhibited 2.06, 1.69 and 4.91 for *Z* ratio in primary hepatocytes, islets and neurospheres, respectively (Fig. 1a). The *Slc12a8* gene belongs to the SLC12 gene family of the electroneutral cation–chloride co-transporters, and the function of the protein encoded by this gene remains unknown[24]. Close homologues exist in mouse, human, zebrafish, *Drosophila* and *Caenorhabditis elegans* (Supplementary Fig. 1a). Although amino acid sequences are significantly diverged, the predicted ten membrane-spanning domains are conserved throughout these Slc12a8 homologues (Supplementary Fig. 1b). *Slc12a8* is highly expressed in the small intestine and pancreas and moderately expressed in the liver and white adipose tissue (Fig. 1b). We confirmed that *Slc12a8* expression was induced significantly in mouse primary hepatocytes, mouse NIH3T3 fibroblasts and ex vivo explants of jejunum and ileum when NAD^+ was reduced by treatment with FK866, whereas this induction was suppressed when NAD^+ was restored by co-administration of FK866 and NMN (Fig. 1c and Supplementary Fig. 1c,d).

To begin to examine whether the *Slc12a8* gene encodes the NMN transporter, we first determined the kinetics of NMN uptake in mouse primary hepatocytes. To inhibit the extracellular degradation of NMN to NR by CD73, the uptake of NR into cells through nucleoside transporters and the intracellular NMN synthesis by NAMPT, we used adenosine-5′-(α,β-methylene)diphosphate (AOPCP), dipyridamole (DIPY) and FK866, respectively. AOPCP inhibits 5′-nucleotidase activity by 97% (Supplementary Fig. 1f). A cocktail of these inhibitors did not affect cell viability up to 30 min (Supplementary Fig. 1e). In the presence of these inhibitors, we added 100 μM NMN and found that intracellular NMN levels significantly increased at the 1 min time point compared with the control in mouse primary hepatocytes (Fig. 1d). In this condition using the same inhibitors and 100 μM NMN, we knocked down *Slc12a8* and *Nrk1*, a major NR kinase that converts NR to NMN intracellularly[10], and examined the uptake of NMN at the 1 min time point in primary hepatocytes. The knockdown efficiencies for both genes are approximately 80% (Fig. 1e). Interestingly, the fast uptake of NMN was completely abrogated in *Slc12a8*-knockdown (*Slc12a8*-KD) hepatocytes, whereas no significant reduction in NMN uptake was observed in *Nrk1*-knockdown (*Nrk1*-KD) hepatocytes (Fig. 1f), suggesting that *Slc12a8* is necessary for the fast uptake of NMN in primary hepatocytes and that the observed increase in intracellular NMN is not due to the conversion of NR or nicotinamide into NMN.

Biochemical features of the Slc12a8 protein. Next, we overexpressed the full-length mouse *Slc12a8* complementary DNA in mouse NIH3T3 cells. We chose this cell line because it does not have any detectable extracellular activities of CD73 (converting NMN to NR) and CD38 (degrading NMN to nicotinamide and phosphoribose) and because it also has very weak NMN uptake activity (see Fig. 2b). The observed molecular weight of the full-length Slc12a8 protein is ~90 kDa, which was also confirmed with amino (N)- and carboxy (C)-terminally FLAG-tagged Slc12a8 proteins (Supplementary Fig. 2a). Slc12a8 protein levels were significantly increased ~2.2-fold in *Slc12a8*-overexpressing NIH3T3 (Slc12a8-OE) cells (Fig. 2a). We then determined the kinetics of NMN uptake using ^{3}H-labelled NMN (^{3}H-NMN) in Slc12a8-OE and control cells. The uptake of ^{3}H-NMN was enhanced with statistical significance at the 3 and 5 min time points in Slc12a8-OE cells compared with control cells (Fig. 2b). Using these Slc12a8-OE cells, we determined the Michaelis–Menten parameters for the Slc12a8 protein. The K_m and the V_{max} for NMN were calculated to be 34.1 ± 8.3 μM and 11.5 ± 1.2 pmol min^{-1} mg^{-1}, respectively (Fig. 2c). Notably, this K_m is consistent with a detected range of NMN concentrations in mouse plasma and erythrocytes[20,25,26]. To further analyse the specificity of Slc12a8, we produced proteoliposomes by combining the membrane fractions of Slc12a8-OE or control NIH3T3 cells with the phospholipid bilayers derived from deproteinized erythrocyte plasma membrane. Slc12a8-OE-derived proteoliposomes incorporated significantly higher (~2-fold) levels of ^{3}H-NMN than those in control-derived proteoliposomes (Supplementary Fig. 2b). Using these Slc12a8-OE proteoliposomes, we examined whether the uptake of ^{3}H-NMN into proteoliposomes would be competed by excess amounts of various cold NAD^+-related compounds. Cold NMN (150 μM) showed complete competition against ^{3}H-NMN uptake, whereas NAD^+, AMP, nicotinic acid mononucleotide (NaMN) and nicotinamide showed minimal or negligible competition at the same concentration (Fig. 2d). We confirmed that NaMN, a structurally very similar compound to NMN, was not transported into Slc12a8-OE proteoliposomes (Supplementary Fig. 2c). Interestingly, 150 μM NR exhibited ~70% displacement (Fig. 2d), and we therefore further determined half-maximum inhibitory concentration (IC_{50}) values for NMN and NR using the proteoliposome system. The IC_{50} for NMN was 22.8 ± 3.6 μM, whereas the IC_{50} for NR was 77.4 ± 10.8 μM (Fig. 2e). This result suggests that the Slc12a8 protein is specific primarily to NMN under physiological conditions, as NR levels have not been shown to reach such high concentrations, such as in blood[22,27] and ascitic exudates[28]. To definitively determine the specificity of Slc12a8 between NMN and NR, we gave doubly labelled, 3-Da-heavier isotopic NMN or NR (O18-D-NMN or O18-D-NR) to Slc12a8-OE and control NIH3T3 cells and measured the amount of these isotopic compounds transported into cells within 5 min. When treating with 25 μM O18-D-NMN, Slc12a8-OE cells showed approximately 4-fold higher uptake of O18-D-NMN compared with control cells but no increase in O18-D-NR, demonstrating unequivocal NMN uptake without any conversion of NMN to NR outside of cells within 5 min (Fig. 2f). In contrast, when treating with 25 μM O18-D-NR, equivalent levels of O18-D-NMN synthesis and equivalent transport of O18-D-NR were detected in Slc12a8-OE and control cells (Fig. 2f). These results clearly demonstrate that Slc12a8 specifically transports NMN, but not NR, in the order of minutes.

Using the Slc12a8-OE proteoliposome system, we next assessed the ion dependency of Slc12a8 for NMN transport. When sodium was replaced with lithium, the ^{3}H-NMN incorporation was dramatically reduced by ~80% (Fig. 2g), indicating that NMN transport by Slc12a8 is sodium ion dependent. Potassium ion is not sufficient to elicit the NMN-transporting function of Slc12a8 (Supplementary Fig. 2d), and chloride ion is not required for NMN transport (Fig. 2g), which distinguishes Slc12a8 from other known Slc12a family members that function as cation–chloride co-transporters[24,29]. Finally, we compared the effect of Slc12a8 overexpression on NAD^+ biosynthesis in NIH3T3 cells. When control and Slc12a8-OE NIH3T3 cells were pre-treated for 1 h with a cocktail of 100 nM FK866, 2 μM DIPY, and 500 μM AOPCP, intracellular NAD^+ levels were significantly reduced in both control and Slc12a8-OE cells (Fig. 2h). However, additional 1 h incubation with 100 μM NMN was able to restore NAD^+ levels to the original levels only in Slc12a8-OE cells, not in control NIH3T3 cells (Fig. 2h). Furthermore, this Slc12a8-mediated restoration of NAD^+ was not affected by WNK463, a specific inhibitor for the WNK kinase that regulates the activity of the cation–chloride co-transporters[29] (Supplementary Fig. 2e). All these results strongly support the function and the specificity of Slc12a8 as a novel NMN transporter in mammals.

In vivo validation of the NMN transporter. To further evaluate the NMN-transporting function of Slc12a8 in vivo, we first knocked down *Slc12a8* in the small intestine, one of the tissues with the

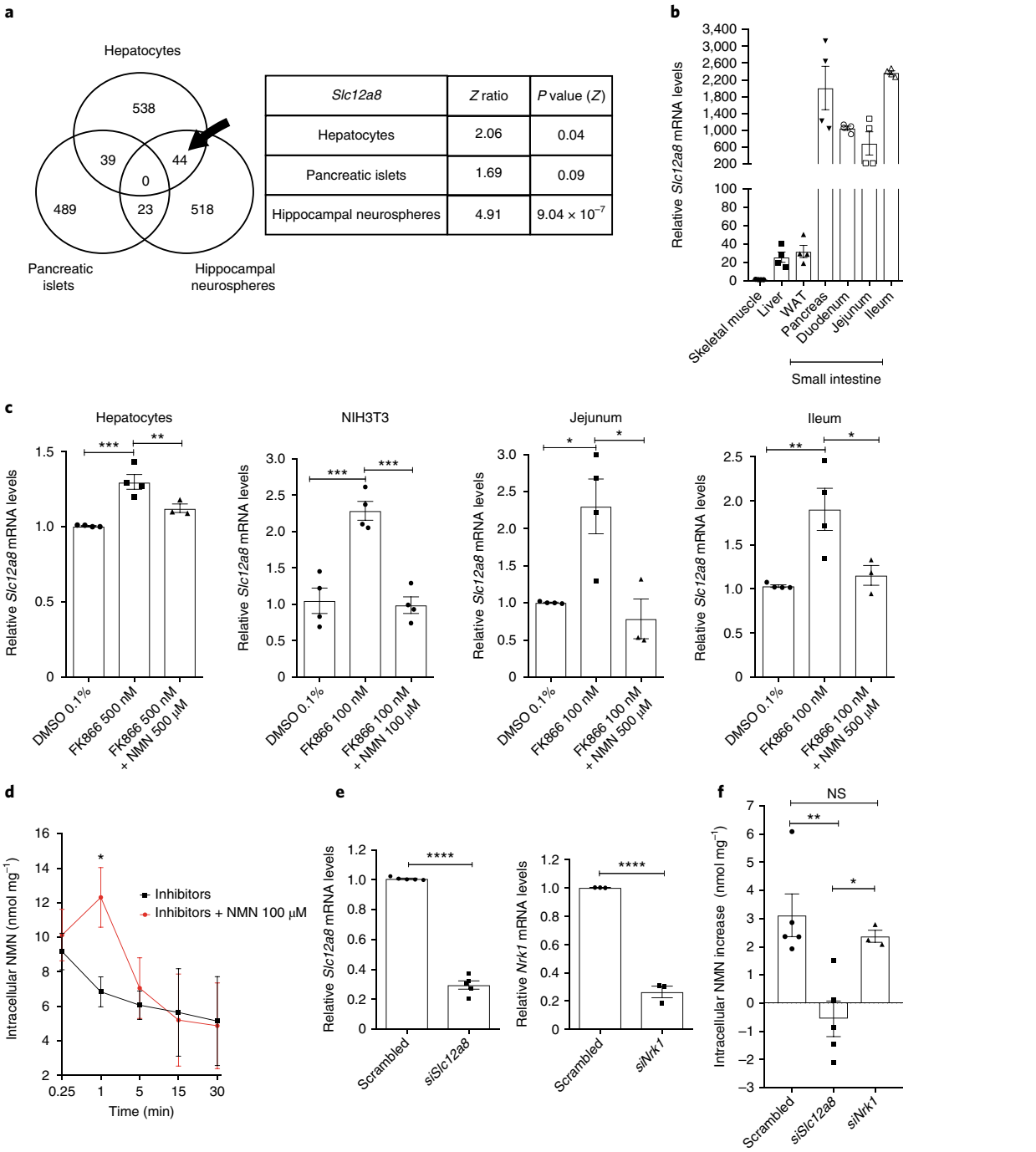

Slc12a8	*Z* ratio	*P* value (*Z*)
Hepatocytes	2.06	0.04
Pancreatic islets	1.69	0.09
Hippocampal neurospheres	4.91	9.04×10^{-7}

Fig. 1 | Identification and characterization of the *Slc12a8* gene. a, Venn diagram of number of genes commonly upregulated in primary hepatocytes, pancreatic islets and hippocampal neurospheres treated with FK866. *Slc12a8* was identified in the section indicated by an arrow. *Z* ratios and two-sided *P* values for *Slc12a8* in each cell type were calculated as described in the Methods ($n=4$ biologically independent samples). **b**, Relative *Slc12a8* mRNA levels in different tissues from B6 male mice at 3 months of age ($n=4$ mice). **c**, Relative *Slc12a8* mRNA levels in primary mouse hepatocytes ($n=4$ mice; $^{**}P=0.0191$, $^{***}P=0.0006$), NIH3T3 fibroblasts ($n=4$ biologically independent samples; DMSO versus FK866 $^{***}P=0.0004$, FK866 versus FK866 + NMN $^{***}P=0.0003$) and ex vivo explants of the jejunum and ileum ($n=4$ mice for DMSO and FK866 alone, $n=3$ mice for FK866 + NMN; jejunum, DMSO versus FK866 $^{*}P=0.0168$ and FK866 versus FK866 + NMN $^{*}P=0.0111$; ileum, DMSO versus FK866 $^{**}P=0.009$ and FK866 versus FK866 + NMN $^{*}P=0.0313$) treated with 0.1% DMSO, FK866 alone or FK866 + NMN (24 h for cells and 4 h for explants; analysed using analysis of variance (ANOVA) with Tukey's test). **d**, Time course of NMN uptake in mouse primary hepatocytes. Hepatocytes were pre-treated with 500 nM FK866 for 24 h and then incubated with a cocktail of 20 µM DIPY, 500 µM AOPCP and 500 nM FK866, with or without 100 µM NMN. NMN was measured by HPLC ($n=4$ mice, except for 3 datasets for the 15 and 30 min time points for inhibitors only; analysed using ANOVA with Sidak's test, $^{*}P=0.0262$). **e**, Knockdown efficiencies of *Slc12a8* and *Nrk1* mRNA in mouse primary hepatocytes ($n=5$ mice for *Slc12a8* silencing, $n=3$ mice for *Nrk1* silencing; analysed by unpaired two-sided *t*-test, *siSlc12a8* $^{****}P<0.0001$, *siNrk1* $^{****}P<0.0001$). **f**, Increases in intracellular NMN content measured by HPLC in primary hepatocytes treated with scrambled, *Slc12a8* and *Nrk1* siRNA at 1 min after addition of 100 µM NMN. Culture conditions were the same as described in **d** ($n=5$ mice for *Slc12a8* silencing, $n=3$ for *Nrk1* silencing; analysed by ANOVA with Tukey's test, $^{**}P=0.0052$, $^{*}P=0.0413$). All values are presented as mean ± s.e.m. NS, not significant; WAT, white adipose tissue.

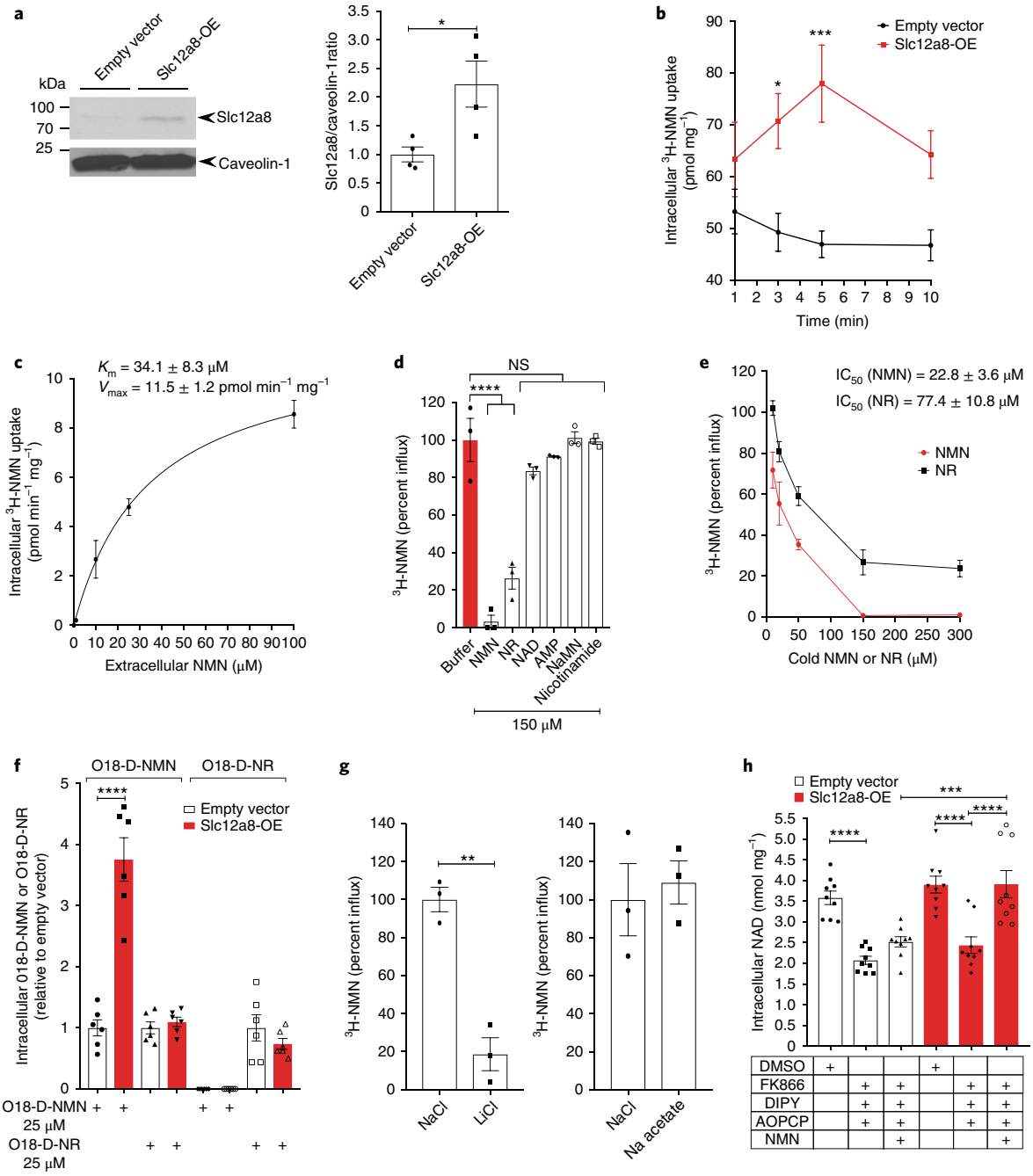

Fig. 2 | The kinetic features of the Slc12a8 NMN transporter and its specificity, sodium dependency and effects on NAD⁺ biosynthesis. a, Slc12a8 protein expression in plasma membrane fractions from control and Slc12a8-OE NIH3T3 cells (left). Slc12a8 protein levels normalized to caveolin-1 protein levels are shown for each cell line (right; $n=4$ independent experiments; analysed by unpaired two-sided t-test, $^{*}P=0.0271$). **b**, Uptake of ^{3}H-NMN (25 μM, 37 °C) in control and Slc12a8-OE NIH3T3 cells ($n=12$ biologically independent samples; analysed by ANOVA with Sidak's test, $^{*}P=0.0136$, $^{***}P=0.0001$). **c**, K_m and V_{max} of Slc12a8 for NMN transport. Those values were determined by non-linear regression analysis by subtracting the backgrounds of control cells ($n=5$ biologically independent samples for 1 and 10 μM, $n=4$ biologically independent samples for 25 and 100 μM). **d**, Substrate specificity of Slc12a8. Transport of ^{3}H-NMN (150 nM, 25 °C) into proteoliposomes derived from Slc12a8-OE cells was measured at 2 min in the presence of competing cold compounds ($n=3$ biologically independent samples; analysed by ANOVA with Dunnett's test, $^{****}P=0.0001$). **e**, The IC_{50} values of NMN and NR. Data are shown as percentages of ^{3}H-NMN uptake ($n=3$ biologically independent samples; IC_{50} was calculated by non-linear regression analysis). **f**, Intracellular levels of O18-D-NMN and O18-D-NR were measured by mass spectrometry in control and Slc12a8-OE NIH3T3 cells incubated with 25 μM O18-D-NMN or O18-D-NR for 5 min ($n=6$ biologically independent samples; analysed by unpaired two-sided t-test, $^{****}P<0.0001$). Values are expressed relative to O18-D-NMN or O18-D-NR levels detected in control NIH3T3 cells. **g**, Ion dependency of NMN uptake by Slc12a8. Sodium ion (Na^+) or chloride ion (Cl^-) was replaced with an equimolar concentration of lithium ion (Li^+) or acetate, respectively ($n=3$ biologically independent samples; analysed by unpaired two-sided t-test, $^{**}P=0.0017$). **h**, Intracellular NAD^+ content was measured as described in the Methods ($n=9$ biologically independent samples; analysed by ANOVA with Tukey's test; control, DMSO versus inhibitors $^{****}P<0.0001$; Slc12a8-OE, DMSO versus inhibitors $^{****}P<0.0001$ and inhibitors versus inhibitors + NMN $^{****}P<0.0001$; control, inhibitors + NMN versus Slc12a8-OE, inhibitors + NMN $^{***}P=0.0002$). All values are presented as mean ± s.e.m. NS, not significant.

highest *Slc12a8* expression levels, by giving oral gavages of lentiviruses carrying control firefly luciferase (*fLuc*) short hairpin RNA (shRNA) or *Slc12a8* shRNA to young wild-type mice. Slc12a8 protein levels were reduced by ~60% in the jejunum and ~50% in the ileum in the mice receiving the *Slc12a8* shRNA–expressing lentivirus in the gut compared with the mice receiving the *fLuc* shRNA–expressing lentivirus (Fig. 3a). When orally administering NMN (500 mg per kg body weight) to those mice, plasma NMN levels significantly increased at 5 min in the control mice, whereas they did not increase at all in the *Slc12a8*-KD mice (Fig. 3b). Instead, plasma nicotinamide levels tended to be higher in *Slc12a8*-KD mice compared with control mice (Fig. 3c), probably because higher levels of NMN were subjected to degradation to nicotinamide in *Slc12a8*-KD mice. Consistent with these results, NAD^+ levels were significantly decreased in the jejunum of *Slc12a8*-KD mice compared with control mice (Fig. 3d). In the ileum, there were small NAD^+ decreases, which did not reach statistical significance, in *Slc12a8*-KD mice (Fig. 3d). These results suggest that Slc12a8 in the small intestine is important for transporting NMN from the gut into the circulation, affecting NAD^+ levels in the small intestine and the systemic NMN supply in vivo.

We also produced whole-body *Slc12a8* knockout (*Slc12a8*-KO) mice by excising exon 4 of the *Slc12a8* gene using the clustered regularly interspaced short palindromic repeats (CRISPR)–CRISPR-associated protein 9 (Cas9) system. The birth ratio of these knockout mice was lower than the expected Mendelian ratio, implying that there was some premature death during the embryonic stage. However, the pups that were born safely were able to grow to adults, and they did not show any gross abnormalities. In these adult *Slc12a8*-KO mice, we confirmed that the expression of the full-length *Slc12a8* messenger RNA was completely abolished in tissues (Supplementary Fig. 3a). We also confirmed that the Slc12a8 protein was abolished in the jejunum, ileum and pancreas of the *Slc12a8*-KO mice by western blotting (Fig. 3e and Supplementary Fig. 3b). The duodenum does not express the Slc12a8 protein (Fig. 3e), even though it expresses high levels of *Slc12a8* mRNA (Fig. 1b). Immunostaining signals of Slc12a8 in the gut, which are detected predominantly in apical, lateral and basal membranes of the villi in the jejunum and ileum of wild-type mice, were abolished in *Slc12a8*-KO mice (Fig. 3f and Supplementary Fig. 3c), confirming the localization of Slc12a8 in the gut epithelia. Consistent with these findings, the *Slc12a8*-KO mice showed significant decreases in NAD^+ levels in the jejunum and ileum, but not in the duodenum, particularly during the dark time when NAD^+ levels usually rise (Fig. 3g and Supplementary Fig. 3d). NAD^+ decreases were also detected in the pancreas during both light and dark times (Supplementary Fig. 3d). To further confirm whether NMN transport is compromised in the small intestine of the *Slc12a8*-KO mice, we conducted a gavage of O18-D-NMN and measured the direct uptake of O18-D-NMN into the jejunum and ileum. At 10 min after administering O18-D-NMN by oral gavage, we clearly detected O18-D-NMN in the wild-type jejunum and ileum, whereas the uptake of O18-D-NMN decreased by 46% and 36% in the jejunum and ileum, respectively, of the *Slc12a8*-KO mice (Fig. 3h).

Lastly, by using primary hepatocytes from control and *Slc12a8*-KO mice, we again compared the transport of O18-D-NMN and O18-D-NR. When treated with 100 μM O18-D-NMN, *Slc12a8*-KO hepatocytes showed ~90% reduction in O18-D-NMN uptake compared with control wild-type hepatocytes at 5 min (Fig. 3i). Both cell types showed no detectable levels of O18-D-NR (Fig. 3i). However, when treating with 100 μM O18-D-NR, equivalent levels of O18-D-NMN synthesis were detected in both *Slc12a8*-KO and control hepatocytes, although there appeared to be some compensatory increases in O18-D-NR uptake in *Slc12a8*-KO hepatocytes (Fig. 3i). These results provide strong support for the specificity and the minute-order kinetics of Slc12a8 as a novel NMN transporter.

***Slc12a8* maintains NAD^+ levels in the aged gut.** It has been well documented that NAD^+ decreases during ageing in multiple tissues[4]. We found that the jejunum and ileum in 24-month-old mice also showed NAD^+ decreases compared with 2-month-old mice, although the difference did not reach statistical significance in the jejunum (Fig. 4a). Consistent with this phenomenon, *Slc12a8* expression was also significantly upregulated in the aged ileum (Fig. 4b). To investigate the biological relevance of this *Slc12a8* upregulation in the aged ileum, we first gave an oral gavage of NMN to young (3-month-old) and aged (26-month-old) wild-type mice. Although the absolute plasma NMN levels were lower throughout all time points in aged mice compared with young mice (Fig. 4c), the fold increases of plasma NMN levels were higher in aged mice compared with young mice (Fig. 4d). After NMN oral gavage, NAD^+ levels were also increased in aged mice to levels close to those observed in young mice (Fig. 4e), and their fold increases were equivalent between young and aged mice (Fig. 4f), indicating that the upregulation of *Slc12a8* plays an important role in counteracting age-associated NAD^+ decline in the small intestine. To further test this possibility, we conducted oral gavages of lentiviruses carrying control *fLuc* shRNA and *Slc12a8* shRNA to 2- and 24-month-old mice and examined their NAD^+ levels in the gut. Knockdown efficiencies were similar between young and aged mice (Supplementary Fig. 4a,b). Significant NAD^+ decreases were detected in the ilea of the aged, but not young, *Slc12a8*-KD mice (Fig. 4g). Luminal NMN content in the jejunum and ileum did not show any significant differences between young and aged mice (Supplementary Fig. 4c). On the contrary, we also overexpressed *Slc12a8* in the small intestine of young wild-type mice by giving oral gavages of the *Slc12a8*-expressing lentivirus. The Slc12a8 protein was overexpressed ~1.5-fold in the ileum (Supplementary Fig. 4d), which induced significant NAD^+ increases there (Supplementary Fig. 4e). Taken together, these results demonstrate that the upregulation of *Slc12a8* in the ileum contributes to the maintenance of NAD^+ levels in the aged intestine.

Discussion

We have previously demonstrated that the transport of NMN from the gut to the circulation and then to tissues occurred within 10 min (ref. [15]). However, the mechanism that mediates such minute-order transport of NMN has so far remained unknown. In this study, we demonstrate that the *Slc12a8* gene encodes a novel NMN transporter in mammals. The mRNA expression of the *Slc12a8* gene is upregulated in response to NAD^+ decline, allowing cells to meet to an urgent demand for NAD^+ biosynthesis. The Slc12a8 NMN transporter is specific to NMN and requires the sodium ion for the transport of NMN. Abrogation or deficiency of *Slc12a8* in cell culture and in the small intestine significantly reduces the uptake of NMN, resulting in reduced NAD^+ levels in the jejunum and ileum in vivo. Conversely, cellular and intestinal overexpression of full-length *Slc12a8* provides a full capacity of NMN transport to the cells that otherwise exhibit minimal NMN transport and increases ileal NAD^+ levels in vivo, respectively. Furthermore, the whole-body *Slc12a8*-KO mice display significant defects in direct, minute-order NMN transport and NAD^+ biosynthesis, particularly in the jejunum and ileum. In the aged ileum, *Slc12a8* expression is upregulated in response to decreased NAD^+ content. Perturbation of this *Slc12a8* upregulation in the aged ileum affects homeostatic regulation of ileal NAD^+, causing further decreased NAD^+ in the aged ileum. Thus, the NMN transporter encoded by the *Slc12a8* gene functions to regulate NMN-driven NAD^+ biosynthesis and maintain intestinal NAD^+ levels in aged individuals.

How NMN is transported into cells has long been a matter of debate in the field of NAD^+ biology. It has been believed that NMN needs to be converted first to NR by CD73 outside of cells, after which NR is transported into cells, likely through the nucleoside

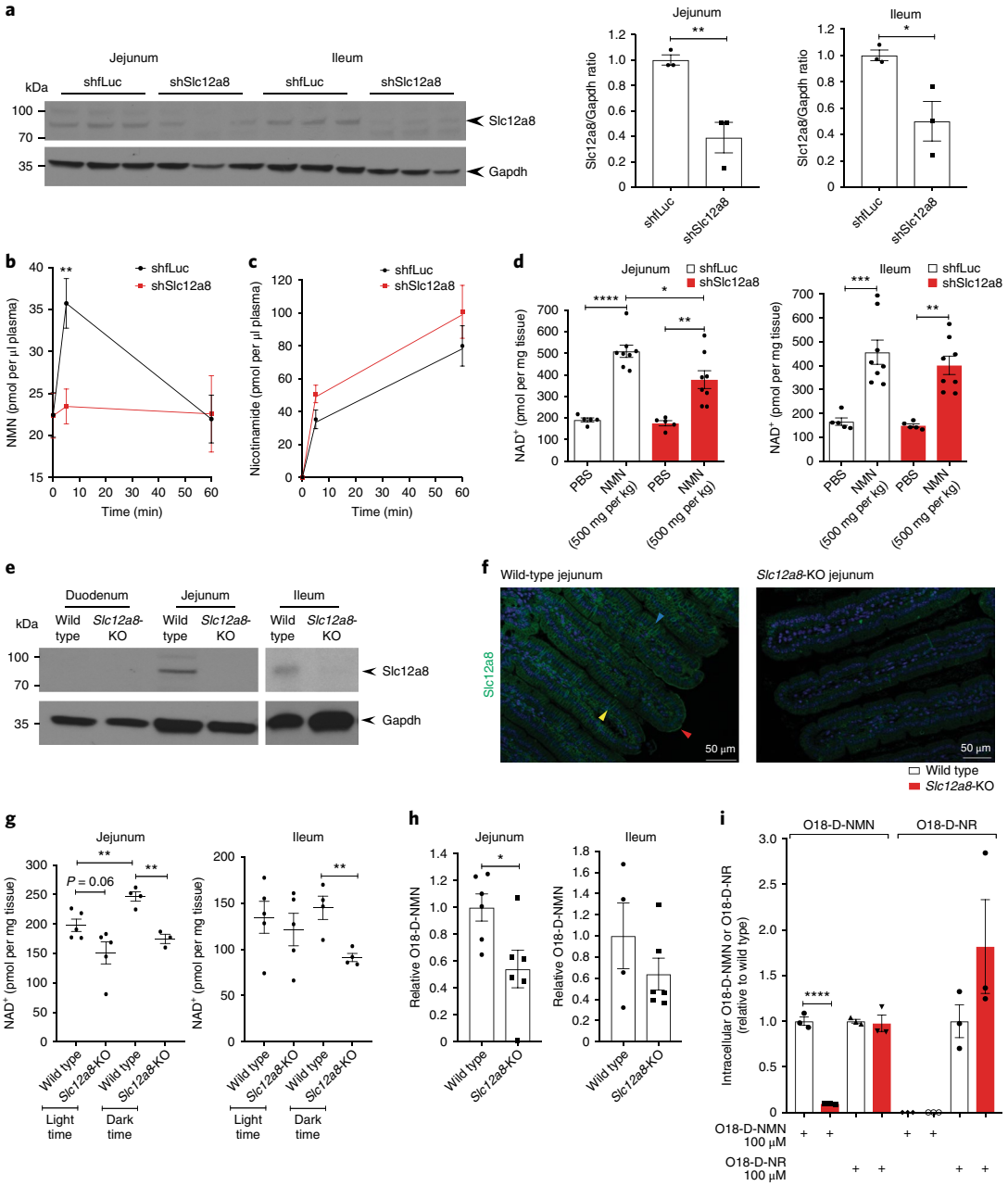

Fig. 3 | In vivo knockdown of *Slc12a8* in the small intestine. a, Slc12a8 protein levels in control and *Slc12a8*-KD jejunum and ileum samples. A representative western blot is shown (left), and bar graphs show Slc12a8 protein levels normalized to Gapdh protein levels (right; $n=3$ mice, repeated twice; B6 males at 3–4 months of age; analysed by unpaired two-sided *t*-test, $^{*}P=0.0324$, $^{**}P=0.0085$). **b**, Plasma NMN levels after an oral gavage of NMN (500 mg per kg body weight) in control and *Slc12a8*-KD mice ($n=6$ mice; B6 males at 3–4 months of age; analysed by ANOVA with Sidak's test, $^{**}P=0.0080$). **c**, Plasma nicotinamide levels in the same mice described in **b** ($n=6$ mice). **d**, Tissue NAD^+ levels in the jejunum and ileum samples collected at the 60 min time point after an oral gavage, as described in **b** ($n=5$ mice for PBS, $n=8$ for NMN; B6 males at 3–4 months of age; analysed by ANOVA with Tukey's test; jejunum, shfLuc PBS versus NMN $^{****}P<0.0001$, shSlc12a8 PBS versus NMN $^{**}P=0.0029$, shfLuc NMN versus shSlc12a8 NMN $^{*}P=0.0029$; Ileum, shfLuc PBS versus NMN $^{***}P=0.0003$, shSlc12a8 PBS versus NMN $^{**}P=0.0030$). **e**, Slc12a8 and Gapdh proteins in tissue lysates of the duodenum, jejunum and ileum of *Slc12a8*-KO mice and wild-type littermates ($n=3$ mice). **f**, Immunostaining of Slc12a8 (green) in the jejunum from 10-month-old *Slc12a8*-KO female mice and wild-type littermates ($n=3$ mice). Red, blue and yellow arrowheads indicate apical, lateral and basal membranes, respectively. Scale bars, 50 µm. **g**, Tissue NAD^+ levels in the jejunum and ileum from *Slc12a8*-KO mice and wild-type littermates, collected during light time (9:00–10:00) or during dark time (21:00–22:00) ($n=5$ mice for the light time, $n=4$ mice for the dark time, except for the 3 data points for the jejunum of Slc12a8-KO mice; females at 8–10 months of age; analysed by unpaired two-sided *t*-test; jejunum, dark time wild type versus *Slc12a8*-KO $^{**}P=0.0015$, light time wild type versus dark time wild type $^{**}P=0.0093$; ileum, dark time willd type versus *Slc12a8*-KO $^{**}P=0.0069$). **h**, Levels of O18-D-NMN in the jejunum and ileum by mass spectrometry at 10 min after orally administering 500 mg per kg of O18-D-NMN in *Slc12a8*-KO mice and wild-type littermates ($n=6$ mice (3 males and 3 females) at 7–8 months of age, except for 2 males and 2 females for the wild-type ileum; analysed by unpaired two-sided *t*-test, $^{*}P=0.0239$). Values are expressed relative to O18-D-NMN levels detected in wild type. **i**, Intracellular levels of O18-D-NMN and O18-D-NR by mass spectrometry in primary hepatocytes isolated from 5-month-old *Slc12a8*-KO male mice and wild-type littermates and incubated with 100 µM O18-D-NMN or O18-D-NR for 5 min ($n=3$ mice; analysed by unpaired two-sided *t*-test, $^{****}P<0.0001$). Values are expressed relative to O18-D-NMN or O18-D-NR levels detected in wild type. All values are presented as mean ± s.e.m.

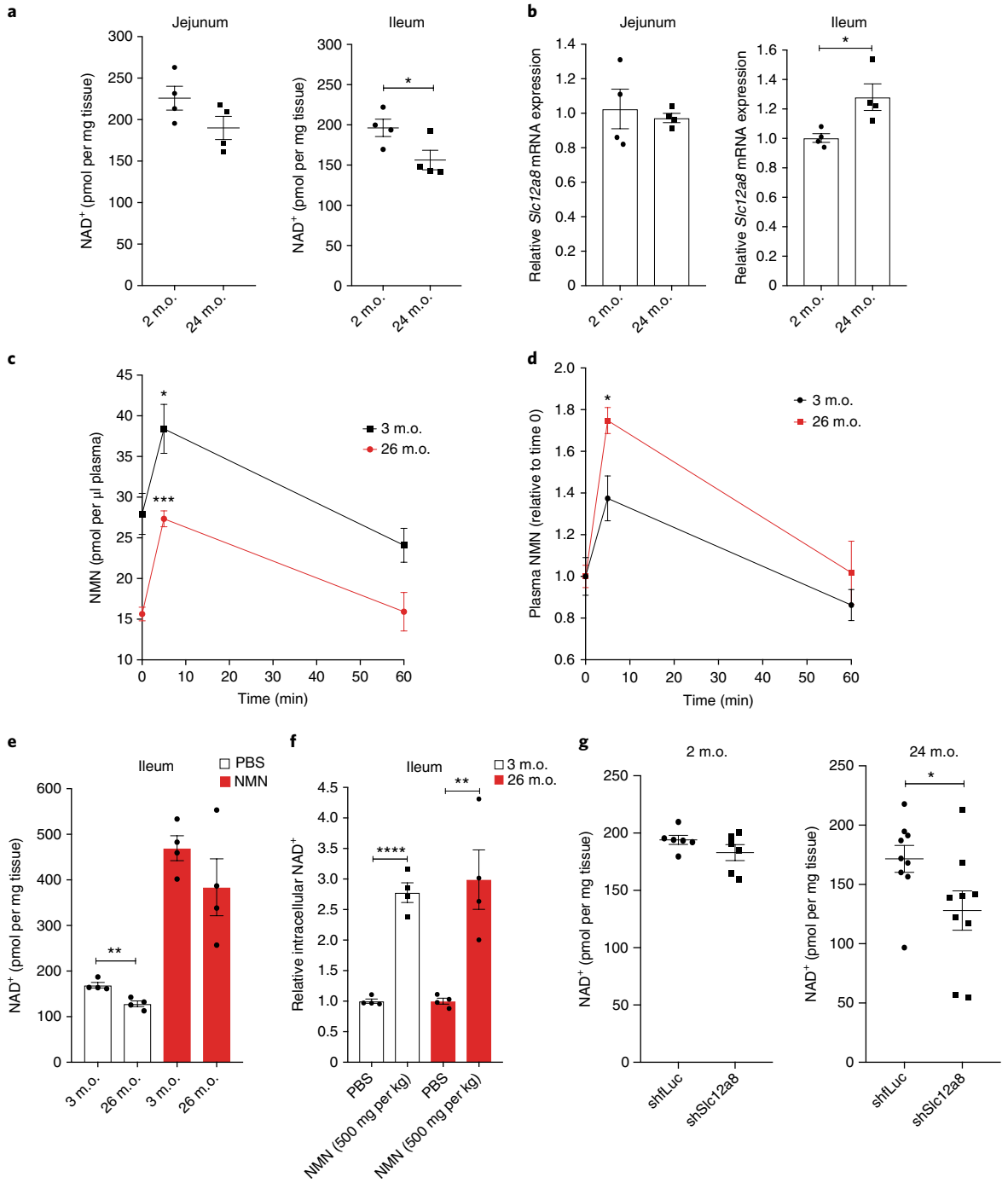

Fig. 4 | The age-associated upregulation of *Slc12a8* in the ileum and its effect on NMN uptake and ileal NAD⁺ biosynthesis in aged mice. a,**b**, NAD⁺ levels (**a**) and relative *Slc12a8* mRNA levels (**b**) in the jejuna and ilea from 2-month-old (2 m.o.) and 24 m.o. B6 female mice. Tissue samples were collected during the dark time (21:00–22:00 ; $n=4$ mice for each age; analysed by unpaired two-sided *t*-test; NAD⁺ levels, $^{*}P=0.0492$; *Slc12a8* mRNA levels, $^{*}P=0.0269$). **c**,**d**, Plasma NMN levels (**c**) and their relative changes (**d**) after an oral gavage of NMN (500 mg per kg body weight) in 3 m.o. and 26 m.o. B6 female mice ($n=4$ mice; analysed by ANOVA with Sidak's test; **c**, $^{*}P=0.0328$, $^{***}P=0.0010$; **d**, $^{*}P=0.0257$). **e**,**f**, Ileal NAD⁺ levels (**e**) and their relative comparisons (**f**) in the ileal samples collected at the 60 min time point after an oral gavage in 3 m.o. and 26 m.o. B6 female mice ($n=4$ mice each for PBS and NMN; analysed by unpaired two-sided *t*-test; **e**, $^{**}P=0.0033$; **f**, $^{**}P=0.0066$, $^{****}P<0.0001$). **g**, NAD⁺ levels in the ilea of 2 m.o. and 24 m.o. control and intestinal *Slc12a8*-KD B6 female mice ($n=6$ mice each for 2 m.o. control and intestinal *Slc12a8*-KD B6 female mice, $n=9$ mice each for 24 m.o. control and intestinal *Slc12a8*-KD B6 female mice; analysed by unpaired two-sided *t*-test, $^{*}P=0.0496$). All values are presented as mean ± s.e.m.

transporter, and reconverted to NMN by NRK1/2 (refs [21,30]). Although this process can occur over the course of 24 h (ref. [21]), such hourly kinetics cannot explain the minute-order uptake of NMN into the cell. Additionally, how to analyse the in vivo kinetics of NMN is also critical, and the results could be significantly affected by differences in sample collection and extraction methodologies[22,23]. For example, plasma samples need to be processed immediately after collection, as we did in this study, because

freezing blood or plasma samples causes inaccurate measures of NMN levels. The results presented in this study strongly indicate that Slc12a8 is specific to NMN, not to NR, and its K_m is consistent with a measured range of NMN concentrations[20,25,26]. Even NaMN, structurally very close to NMN, cannot be transported by Slc12a8. Furthermore, its dependency on sodium ion, but not chloride or potassium ions, and its insensitivity to WNK463 distinguish Slc12a8 from other known cation–chloride co-transporters. Nonetheless, because a very high, supra-physiological concentration of NR can compete against NMN, NR might be able to interact with Slc12a8 weakly. To elucidate the precise details of the structure–function relationship between Slc12a8 and NMN, it will be of great importance to determine the crystal structure of the Slc12a8 NMN transporter.

The results from gut-specific *Slc12a8*-KD mice and whole-body *Slc12a8*-KO mice demonstrate that the major place where NMN is absorbed is the small intestine, particularly the jejunum and ileum. Whereas we can detect NMN in the luminal content of the jejunum and ileum, the source of NMN remains unknown. For humans, a source may be certain vegetables and fruits that contain NMN[15]. Additionally, it has been reported that human and cow milk contains NMN at micromolar concentrations[31,32]. For mice, one interesting possibility is that NMN could be produced from the enzymatic degradation of NAD^+ in the small intestine. Another possibility is that certain gut bacterial species may produce NMN. If this is the case, the Slc12a8 NMN transporter would likely play a critical role in the symbiotic regulation of NAD^+ biosynthesis between the microbiota and the host.

Remarkably, the function of the Slc12a8 NMN transporter becomes crucial in aged individuals compared with young ones. In response to significant decreases in NAD^+ levels, the aged ileum upregulates *Slc12a8* expression and tries to maintain its NAD^+ levels. When enough NMN is supplied, this feedback system can function adequately to maintain levels of NAD^+ comparable to those in young ilea. Therefore, increasing NMN availability or stimulating the function of the NMN transporter could effectively counteract age-associated NAD^+ decline in the aged small intestine. In addition to ageing, the NMN-transporting function of Slc12a8 might also be important for the pathogenesis of some diseases. For example, the human *SLC12A8* gene has been identified as a psoriasis susceptibility candidate gene[33]. Most recently, it has been reported that the high expression levels of *SLC12A8* and its genetic polymorphism are associated with better prognosis for patients with pancreatic ductal adenocarcinomas[34] and breast cancers[35], respectively. Thus, the Slc12a8 NMN transporter could be a new, interesting target for pharmaceutical drug development.

In conclusion, the identification and the characterization of the Slc12a8 NMN transporter further advances our understanding of the physiological importance of NMN as a key systemic NAD^+ intermediate. Because NMN conveys remarkable effects of mitigating age-associated physiological decline in mice[4,15], identifying compounds that could promote the NMN-transporting function of the Slc12a8 protein will provide an interesting opportunity to develop a more effective anti-ageing intervention, combined with NMN administration.

Methods

Microarray analysis. Total RNA was isolated from primary hepatocytes, pancreatic islets and hippocampal neurospheres treated with 0.1% DMSO (control) or FK866 (200 nM for primary hepatocytes and 10 nM for pancreatic islets and hippocampal neurospheres). Primary hepatocytes and pancreatic islets were isolated from 3-month-old C57BL/6J (B6) male mice (Jackson Laboratories). To determine transcriptional changes induced by FK866 treatment, microarray analyses were conducted using Illumina MouseRef-8 (v.2) whole-genome microarrays. The background-subtracted raw microarray data were subjected to *Z* score transformation, and *Z* ratios were calculated as described previously[5]. Z ratios were calculated by taking the difference between the averages of the observed gene Z scores and dividing it by the standard deviations of all of the differences for that particular comparison. All data were analysed by the R statistical software package.

Cell culture and ex vivo small intestine explant culture. NIH3T3 cells (originally purchased from the American Type Culture Collection) were cultured at 37 °C and 5% CO_2 in DMEM supplemented with 10% FBS, 100 units ml^{-1} penicillin and 100 μg ml^{-1} streptomycin. For *Slc12a8* mRNA expression analysis, 2.5×10^5 cells per well were incubated for 24 h in 6-well plates in DMEM supplemented with 1% FBS containing 0.1% DMSO, 100 nM FK866 or 100 nM FK866 plus 100 μM NMN. Small intestines from 3-month-old B6 male mice (Jackson Laboratories) were cut into three segments with duodenum:jejunum:ileum length ratios of 1:3:2 (ref. [36]). From each segment, 1 cm was opened longitudinally, washed once with cold PBS and incubated in the medium described below for 4 h at 37 °C supplemented with 0.1% DMSO, 100 nM FK866 or 100 nM FK866 plus 500 μM NMN. The medium was a 1:1 mixture of DMEM and Ham's F-12 medium (Sigma-Aldrich) with 5% FBS and the following additives: 5 μg ml^{-1} insulin (Sigma-Aldrich), 20 ng ml^{-1} epidermal growth factor (Sigma-Aldrich), 1× B27 supplement (GIBCO), 1 mM sodium pyruvate (Corning), 100 units ml^{-1} penicillin, 100 μg ml^{-1} streptomycin and 2 mM glutamax (GIBCO). Cellular and tissue total RNA samples, which were extracted using the PureLink RNA Mini kit (Ambion), were analysed by quantitative RT–PCR, and relative expression levels were calculated for each gene by normalizing to *Gapdh* expression levels[16].

NAD^+ and NMN measurements by HPLC. NAD^+ and NMN were extracted from cells and tissues with perchloric acid, neutralized with K_2CO_3 on ice and quantitated by our HPLC system (Shimadzu) with a Supelco LC-18-T column (15 cm × 4.6 cm; Sigma-Aldrich) and a Hypercarb column (15 cm × 4.6 cm; Thermo Fisher Scientific), respectively[5,37].

Flow cytometry analysis. NIH3T3 cells (2×10^6) were incubated for 48 h at 37 °C and 5% CO_2 in a 10-cm culture dish in DMEM supplemented with 1% FBS containing 0.1% DMSO, 100 nM FK866 or 100 nM FK866 plus 100 μM NMN. Cells were then washed once with cold PBS, treated with 0.02% EDTA in PBS and stained for flow cytometry using a commercially available polyclonal rabbit antibody to mouse Slc12a8 at 1:200 (ARP44039, Aviva), a secondary goat antibody to rabbit immunoglobulin G (H + L) conjugated with Alexa Fluor 488 at 1:2,000 (Invitrogen) and the survival marker Zombie Dye at 1:400 (BioLegend) for 25 min at 4 °C. Cells were then washed and analysed by the Gallios Flow Cytometer (Beckman Coulter). For the intracellular staining, cells were first fixed in 2% PFA for 10 min at room temperature and then permeabilized in saponin-containing buffer for another 10 min at room temperature. Slc12a8 staining was performed in permeabilization buffer for 25 min at 4 °C. Samples were analysed by the Gallios Flow Cytometer, and data were analysed using Kaluza v.1.3 (Beckman Coulter). Dead cells were excluded using a Zombie Aqua Fixable Viability Kit (BioLegend).

Hepatocyte isolation, 5′-nucleotidase activity assay, NMN uptake measurement and silencing of *Slc12a8* and *Nrk1* expression. Primary hepatocytes were isolated from 3-month-old B6 male mice (Jackson Laboratories) by a two-step hepatic portal perfusion with calcium- and magnesium-free Hanks' salt solution followed by DMEM containing 0.25 mg ml^{-1} collagenase (Type IV; Sigma-Aldrich)[38]. Cells were cultured overnight in 6-well plates coated with poly-L-lysine at 37 °C and 5% CO_2 in DMEM supplemented with 10% FBS, 100 units ml^{-1} penicillin and 100 μg ml^{-1} streptomycin before conducting any experiments. *Slc12a8* mRNA expression and NAD^+ content were evaluated by incubating hepatocytes with 500 nM FK866 or 500 nM FK866 plus 500 μM NMN in DMEM with 1% FBS for 24 h. To confirm whether AOPCP inhibits 5′-nucleotidase activity, 1.5×10^5 cells per well were grown in 12-well plates with 500 nM FK866 in DMEM with 1% FBS for 24 h and then incubated in 1.4 ml Hanks' buffered saline solution with Ca^{2+} and Mg^{2+} at pH 7.5 (HBSS; GIBCO) in the presence of 100 μM AMP or 100 μM AMP plus 500 μM AOPCP. At different time points (0, 1, 5, 15 and 30 min), 200 μl of each culture supernatant was collected and extracted by adding 28 μl 70% perchloric acid. The amounts of adenosine produced were determined by HPLC. Elution times for AMP and adenosine were 4.7 and 17.4 min, respectively. To examine cell viability, CellTiter 96 AQueous One Solution Cell Proliferation Solution (Promega) was used, and the absorbance was measured at $\lambda = 490$ nm after 4 h incubation. For NMN uptake measurement, 1.5×10^5 cells per well were grown in 12-well plates with 500 nM FK866 in DMEM with 1% FBS for 24 h and then incubated in 1 ml of HBSS in the presence of 500 μM AOPCP, 20 μM DIPY and 500 nM FK866 or these inhibitors plus 100 μM NMN. At different time points (0, 0.25, 1, 5, 15 and 30 min), cells were washed once with cold HBSS and lysed in cold 10% perchloric acid. Intracellular NMN levels were measured by HPLC, as described previously[5]. For gene silencing experiments, 10 μg of ON-TARGETplus mouse siRNA (Thermo Fisher Scientific) specific to *Slc12a8* (J-042450-12-0020) or *Nrk1* (J-051839-11-0010) or a negative control siRNA (non-targeting siRNA number 1, D-001810-01-20) was electroporated into 1 million cells per condition, mixed with 100 μl AMAXA Mouse Hepatocyte Nucleofector Solution (Lonza), using the Nucleofector programme H-26 following the manufacturer's instructions. The electroporated cells were incubated in the cuvette for 15 min before addition of medium. Cells (2.5×10^5 per well) were seeded in 6-well plates coated with poly-L-lysine at 37 °C

and 5% CO_2 in DMEM containing 10% FBS and penicillin–streptomycin for 48 h after electroporation. Those cells were incubated with 500 nM FK866 in DMEM with 1% FBS for 24 h. NMN uptake was measured by HPLC after incubating cells in HBSS with 500 μM AOPCP, 20 μM DIPY and 500 nM FK866 or these inhibitors plus 100 μM NMN for 1 min at room temperature. Silencing efficiencies were evaluated by quantitative RT–PCR.

Generation of NIH3T3 cells stably overexpressing the full-length mouse *Slc12a8* complementary DNA. The coding region of full-length mouse *Slc12a8* cDNA (GenBank reference sequence NM_134251) was amplified from mouse liver by PCR using PfuUltra II Fusion HS DNA polymerase (Agilent) with the following forward and reverse primers containing XhoI sites: *Slc12a8* forward, 5′-ATACTCGAGGAGAATGGCCCAGAGGTCTC-3′; *Slc12a8* reverse, 5′-TCAACTACGGAGGGATGATCGAGCTCATT-3′. The resulting 2,118–base pair (bp) fragment of full-length *Slc12a8* cDNA was digested with XhoI and cloned into pBluescript SK(−) vector. The *Slc12a8* cDNA fragment was then subcloned into the mammalian expression vector pCXN2 (ref. [39]). N- or C-terminally FLAG-tagged versions of full-length *Slc12a8* cDNA were produced using the following forward and reverse primer sets containing XhoI sites and FLAG-tag sequences: N-terminally FLAG-tagged *Slc12a8*, forward, 5′-ATACTCGAGCCACCATGGACTACAAAGACGATGACGACAA-GGGCGCCCAGAGGTCTCCG-3′; N-terminally FLAG-tagged *Slc12a8*, reverse, 5′-TCAACTACGGAGGGATGATCGAGCTCATT-3′; C-terminally FLAG-tagged *Slc12a8*, forward, 5′-ATACTCGAGCCACCATGGCCCAGAGGTCTCCG-3′; C-terminally FLAG-tagged *Slc12a8*, reverse, 5′-TCAACTACGGAGGGATGCCGC TGATGTTTCTGCTACTGCTGTTCATCGAGCTCATT-3′.

The resultant FLAG-tagged *Slc12a8* cDNA fragments were cloned into the mammalian expression vector pIRES-EGFP-puro (catalogue number 45567; Addgene). The *Slc12a8* cDNA sequence in the final vector was confirmed by sequencing. In one set of experiments, NIH3T3 cells were transfected with 5 μg of pCXN2carrying the full-length *Slc12a8* cDNA (Slc12a8-OE) or only pCXN2 vector (control) using the SuperFect transfection reagent (Qiagen) and cultured inDMEM supplemented with 10% FBS, antibiotics and 300 μg ml^{-1} G418(Invitrogen) for 2 weeks. In another set of experiments, NIH3T3 cells were transfected with 5 μg of pIRES-EGFP-puro carrying the full-length *Slc12a8* cDNAwith N- or C-terminal FLAG-tag (N- or C-FLAG Slc12a8-OE) or only pIRES-EGFP-puro vector (control) using the SuperFect transfection reagent (Qiagen) and cultured in DMEM supplemented with 10% FBS, antibiotics and 1 μg ml^{-1} puromycin (Sigma-Aldrich) for 2 weeks. Resistant cells were pooled, andaliquots were frozen for further experiments. To confirm Slc12a8 protein expression levels, plasma membrane fractions were prepared from control and Slc12a8-OE cells or from N- or C-FLAG Slc12a8-OE cells, as described previously[40]. Briefly, 7.5×10^7 cells were cultured in 5 10-cm dishes. After two washes with ice-cold HES buffer (20 mM HEPES, 1 mM EDTA and 255 mM sucrose pH 7.4), cells were collected by scraping in HES buffer (3 ml per dish) containing a protease inhibitor cocktail (Roche) and were homogenized by being passed five times through a 22-gauge needle. All subsequent steps were performed at 4 °C. The homogenate was centrifuged (Avanti J-E; Beckman Coulter) at 10,000*g* in a JA-25.5 rotor for 15 min. The resulting supernatant was layered on the top of a 10-ml sucrose cushion (38.5% sucrose, 20 mM HEPES and 1 mM EDTA; pH 7) and centrifuged at 53,000*g* for 120 min. The interface containing the plasma membrane fraction was carefully removed, resuspended in 10 ml HES buffer and centrifuged at 50,000*g* for 30 min, yielding the plasma membrane fraction in the pellet. Plasma membrane fractions from control or Slc12a8-OE cells were lysed with RIPA buffer (150 mM sodium chloride, 1.0% NP-40, 0.25% sodium deoxycholate, 0.1% SDS, 50 mM Tris pH 7.5, 2 mM EDTA, 1 mM PMSF, 0.5 mM DTT and protease inhibitor cocktail) and boiled for 5 min in 1× Laemmli buffer. Western blotting was conducted with polyclonal rabbit anti–mouse Slc12a8 (1:500; ARP44039; Aviva) or monoclonal anti-FLAG M2 (1:500; F3165; Sigma-Aldrich) and anti-caveolin-1 (1:2,000; 3238; Cell Signalling). Band intensity was quantitated on the Amersham Hyperfilm ECL (GE Healthcare) by Photoshop. To measure intracellular NAD^+ levels, 2×10^5 control and Slc12a8-OE NIH3T3 cells were preincubated with 2 μM DIPY, 500 μM AOPCP, 100 nM FK866 and, in some experiments, 10 μM WNK463, a pan-WNK kinase inhibitor (MedChemExpress), for 1 h and then with the same inhibitors combined with 100 μM NMN for an additional 1 h in DMEM supplemented with 1% FBS at 37 °C. At the end of incubation, cells were washed once with cold PBS and lysed in 10% perchloric acid. NAD^+ levels were determined by HPLC, as described above.

NMN uptake analyses with radiolabelled NMN. Control and Slc12a8-OE NIH3T3 cells were collected by centrifugation (400*g*, 5 min), washed once in HBSS and incubated at 37 °C in HBSS pH 7.5 (5×10^6 cells ml^{-1}) containing 100 nM ^{3}H-β-NMN (9 Ci $mmol^{-1}$; Moravek Biochemicals) and unlabelled NMN to make the final concentration 25 μM. At the designated time points (1, 3, 5 and 10 min), aliquots of the cells (100 μl) were collected and placed in 1.5 ml microcentrifuge tubes containing silicone–mineral oil (density, 1.015; Sigma-Aldrich) on the top of 2 M potassium hydroxide solution, followed by centrifugation at 16,000*g* for 30 s. Cells were separated from the buffer and pelleted through the silicone–mineral oil layer. The radioactivity in these cell pellets was determined by a liquid scintillation counter. For calculating K_m and V_{max}, we used the same condition described above, but with various total concentrations of NMN, ranging from 1 μM to 100 μM. At the 4 min time point, 100 μl of cell suspension was collected and pelleted in the same way described above. The radioactivity in cell pellets was determined by a liquid scintillation counter. The radioactivity measured in control NIH3T3 cells was subtracted to calculate Slc12a8-specific NMN uptake in Slc12a8-OE NIH3T3 cells.

Proteoliposome experiments. Proteoliposome preparation was carried out as previously described[41]. Briefly, 2×10^7 control or Slc12a8-OE NIH3T3 cells were resuspended in 1 ml lysis buffer (10 mM Tris–HCl pH 8.3, 150 mM NaCl, 0.3 M sucrose, protease inhibitor cocktail) and disrupted using a homogenizer. The lysate was centrifuged for 10 min at 3,000*g*, and the supernatant was collected and centrifuged for 15 min at 100,000*g*. The membrane proteins were solubilized with buffer A (10 mM Tris–HCl pH 8.3 containing 150 mM NaCl and 0.5% *n*-octyl-β-glucopyranoside). Separately, total lipids were extracted from haemoglobin-free erythrocyte membranes (ghosts), as described previously[42]. Total lipids from human erythrocyte membranes (3 mg) were dried and resuspended with 600 μl of solubilized membrane proteins (at approximately 0.7 mg ml^{-1} protein concentration). The resulting emulsions were sonicated in ice for 1 min and dialysed against 5 l of buffer A without *n*-octyl-β-glucopyranoside (dialysis buffer) for 24 h at 4 °C. Proteoliposomes were recovered, centrifuged for 15 min at 100,000*g*, resuspended in 900 μl dialysis buffer and passed 5 times through a 30-gauge needle. To examine the Na^+, K^+ or Cl^- dependency of Slc12a8, NaCl was replaced with 150 mM LiCl, KCl or CH_3COONa, respectively. All steps were carried out at 4 °C. Proteoliposomes (30 μl in triplicate for each condition) were incubated for 2, 5 and 10 min at 25 °C in the presence of 150 nM (10^5 cpm ml^{-1}) ^{3}H-β-NMN (specific activity, 9.1 Ci $mmol^{-1}$) with or without 150 μM label-free compounds (NMN, NR, NAD, AMP, NaMN and nicotinamide). At the end of incubations, samples were filtered on a glass fibre paper. Filters were washed with 3 ml of dialysis buffer, dried and counted for radioactivity. In each experiment, we always measured the non-specific binding/uptake of ^{3}H-NMN by adding 150 nM ^{3}H-NMN and 300 μM cold NMN (2,000-fold higher concentration) to the proteoliposomes derived from Slc12a8-OE NIH3T3 cells and measuring the radioactivity of ^{3}H-NMN after extensive washes. Because specific NMN transport should be displaced completely by the 2,000-fold higher concentration of cold NMN, ^{3}H-NMN detected in this condition must be due to a non-specific/non-kinetic transport and/or a non-specific binding to proteoliposomes. Such values due to non-specific transport/binding of ^{3}H-NMN were always measured in each experiment and subtracted from all measured values of ^{3}H-NMN transported into proteoliposomes in each condition. To examine whether Slc12a8 could transport NaMN, proteoliposomes (300 μl in triplicate for each condition) were incubated for 5 min with 5 mM NMN or NaMN (Sigma-Aldrich). Right after incubation, samples were filtered on a glass fibre paper (0.25 cm^2 area), and nucleotides were extracted with 200 μl of 0.6 M perchloric acid. Extracts were neutralized with 2 M K_2CO_3, and nucleotides were quantitated by HPLC.

In vivo *Slc12a8* knockdown and overexpression. To generate shRNA-expressing lentiviral constructs, 56-bp double-stranded oligonucleotides, each of which contained a sense target sequence, a microRNA-based loop sequence (CTTCCTGTCA), an antisense sequence, a termination sequence of four thymidines and appropriate restriction enzyme sites at both ends, were generated for mouse *Slc12a8* and *fLuc* and cloned into the U6-PGK-GFP vector provided by the Viral Vectors Core at Washington University School of Medicine. The sense *Slc12a8* sequence is 5′-GCCTAGAGTGAACAGAGAAGA-3′. To generate the *Slc12a8*-expressing lentiviral construct, a 2,118-bp fragment of full-length *Slc12a8* cDNA was subcloned into the FCIV.FM1 vector provided by the Viral Vectors Core. Lentiviruses were produced by co-transfecting HEK293T cells with the shRNA- or *Slc12a8*-expressing vectors and three packaging vectors (pMD-Lg, pCMV-G and RSV-REV) using SuperFect transfection reagent (Qiagen). Culture supernatant was collected 48 h after transfection[43]. Knockdown or overexpression efficiencies were tested using primary intestinal cultures[44]. Large-scale lentivirus production was carried out by the Viral Vectors Core at the Hope Center for Neurological Disorders at Washington University. After an overnight fast for two consecutive days, C57BL/6J mice (Jackson Laboratories) orally received *fLuc* or *Slc12a8* shRNA lentivirus with a titre of 5×10^6 transduction units, or vector-only or Slc12a8-expressing lentivirus with a titre of 3×10^6 transduction units.

Generation of antibodies against mouse Slc12a8 and tissue western blot analysis. Two different polyclonal rabbit antisera were produced against a synthesized N-terminal peptide (AQRSPQELFHEAAQQGC) of mouse Slc12a8 (Covance). Mouse tissues were homogenized with RIPA buffer and boiled in 1× Laemmli buffer for 5 min. Western blotting was conducted with a rabbit polyclonal antiserum against the N-terminal portion of mouse Slc12a8 (1:500; Covance) and an anti-Gapdh antibody (1:1,000; MAB374; Millipore). Band intensity was quantitated on the Amersham Hyperfilm ECL (GE Healthcare) by Photoshop.

Generation of the whole-body *Slc12a8*-KO mice. Whole-body *Slc12a8*-KO mice were generated with the CRISPR-CAS9 technology by the Transgenic Vectors Core

of Washington University. CRISPR gRNAs were designed to flank exon 4 of the *Slc12a8* gene. gRNA sequences were as follows: 5′ gRNA; 5′-agtgcatgtatagacgtatg-3′ and 3′ gRNA; 5′-cctcacaaatatttacaggc-3′. gRNAs were obtained as gBlocks (IDT). Cleavage activity was assessed by transfecting N2A cells with gBlock and Cas9 plasmid (addgene # 42230) using XtremegeneHP (Roche). Cleavage activity was determined by T7E1 assay using standard methods. gRNA was *in vitro* transcribed using the T7 Megashort Script Kit (Ambion). Cas9 RNA was *in vitro* transcribed using the mMessage mMachine T7 Ultra Kit (Ambion). All RNA was purified using Megaclear Columns (Ambion). RNA was microinjected into C57BL/6 J × CBA hybrid zygotes at a concentration of 50 ng/µl Cas9, 25 ng/µl gRNA, and 100 ng/µl ssODN in the Washington University Mouse Genetic Core Facility. Whole-body knockout alleles were detected by PCR across the cleavage site and confirmed by sequencing. One heterozygous founder was established, and the mice were backcrossed to wild-type C57BL/6 J mice (Jackson Laboratories) for 5 generations before analysis. *Slc12a8*-deficient heterozygous mice were crossed to generate homozygous Slc12a8-KO mice. Wild-type littermates were used as controls.

Production of O18-D-NR and O18-D-NMN. ^{18}O-nicotinamide was prepared from the hydrolysis of cyanopyridine in ^{18}O water[45]; 1,2-^{2}H,3,5-tetraacetate was synthesized from D-[2-^{2}H]-ribose (purchased from Omicron Biochemicals)[46]. ^{18}O-^{2}H-labelled NR (O18-D-NR) was synthesized from ^{18}O-nicotinamide and D-ribofuranose 1,2-^{2}H,3,5-tetraacetate[47]. ^{18}O-^{2}H-labelled NMN (O18-D-NMN) was synthesized from O18-D-NR as described previously[15].

Isotopic tracing experiment. Primary hepatocytes (3×10^5) isolated from 5-month-old male *Slc12a8*-KO mice and their wild-type littermates were incubated in 6-well plates with 100 µM O18-D-NMN or O18-D-NR in DMEM with 1% FBS for 5 min at 37 °C. Control and Slc12a8-OE NIH3T3 cells (3×10^5) were incubated in 6-well plates with 25 µM O18-D-NMN or O18-D-NR in DMEM with 1% FBS for 5 min at 37 °C. After incubation, cells were washed twice with cold PBS and lysed in a cold 1:1 mixture of reagent-grade methanol and water. *Slc12a8*-KO mice and their wild-type littermates (7–8 months old) were orally administered O18-D-NMN at a dose of 500 mg per kg or PBS after an overnight fast. The jejunum and ileum were collected at 10 min after oral gavage. A 1:1 mixture of reagent-grade methanol and water (4 °C) was added to the frozen tissue (60 µl per mg tissue). After sonication, extracts were centrifuged at 12,000 *g* for 15 min at 4 °C. Chloroform was added to the extracts at a ratio of 1:1 (v/v), thoroughly shaken for 30 s and centrifuged at 12,000*g* for 10 min at 4 °C. The upper phase (methanol and water) was separated from the lower (organic) phase and lyophilized by speed vacuum at room temperature, reconstituted with 5 mM ammonium formate and centrifuged at 12,000*g* for 10 min. Serial dilutions of NMN, O18-D-NMN and O18-D-NR at concentrations ranging from 128 to 1,000 nmol l^{-1} in 5 mM ammonium formate were used for calibration. Liquid chromatography was performed by HPLC (1290; Agilent) with Atlantis T3 (LC 2.1 × 150 mm, 3 mm; Waters) at a flow rate of 0.15 ml min^{-1} with 5 mM ammonium formate for mobile phase A and 100% methanol for mobile phase B. Metabolites were eluted with gradients of 0–10 min, 0–70% B; 10–15 min, 70% B; 16–20 min, 0% B. The metabolites were analysed with a triple quadrupole mass spectrometer (6470; Agilent) under positive electrospray ionization multiple reaction monitoring using parameters for NMN (335 > 123), O18-D-NMN (338 > 125) and O18-D-NR (258 > 125). Fragmentation, collision and post-acceleration voltages were 135 V, 8 V and 7 V for NMN and 130 V, 20 V and 1 V for NR. Peaks of NMN, O18-D-NMN, and O18-D-NR were identified using the MassHunter quantitative analysis tool (Agilent). The areas under the peaks of O18-D-NMN and O18-D-NR were calculated by subtracting the background values of PBS controls.

Animal experimentation. All mice were group-housed in a barrier facility with 12-h light/12-h dark cycles. Mice were maintained ad libitum on a standard chow diet (LabDiet 5053; LabDiet). For plasma NMN kinetics and tissue NAD$^+$ detection, 3- to 4-month-old male C57BL/6J mice (Jackson Laboratories) that received an oral gavage of *fLuc* or *Slc12a8* shRNA lentivirus as well as 3-month old and 26-month-old female C57BL/6J mice (Charles River) were fasted overnight. Blood was collected from their tail veins at 0, 5 and 60 min after an oral gavage of NMN (500 mg per kg) or PBS. Immediately after blood collection, plasma was separated and quickly extracted with perchloric acid. At this step, it is critical to avoid freezing plasma samples. To show the importance of this procedural precaution, we gave an oral gavage of O18-D-NMN to 7-month-old male C57BL/6J mice (Jackson Laboratories) and measured O18-D-NMN (M + 3), O18-NMN (M + 2), and NMN (M + 0) at 5 min by extracting plasma samples freshly (without freezing/thawing). In this experimental condition, we were able to detect O18-D-NMN (M + 3) reliably in plasma samples at 5 min after oral gavage (Supplementary Fig. 4f), which differs from recently reported results[23]. Indeed, extraction of NR from human plasma samples also requires similar caution[22]. Tissue samples were also collected at 60 min time points after an oral gavage of NMN (500 mg per kg) or PBS. NAD$^+$ levels and *Slc12a8* mRNA expression were determined in tissues from 2-month-old or 24-month-old female C57BL/6J mice (Jackson Laboratories) or those in which *Slc12a8* was knocked down specifically in the small intestine, as described above. Luminal NMN content was compared by mass spectrometry in the jejunum and ileum between 3-month-old and 26-month-old female C57BL/6J mice (Charles River) fasted overnight. All animal studies were approved by the Washington University Institutional Animal Care and Use Committee and were in accordance with National Institutes of Health guidelines.

Immunostaining of Slc12a8 in the small intestine. Jejuna and ilea were prepared by the Swiss-roll method and fixed overnight in 10% buffered formalin (Sigma-Aldrich). Fixed tissues were dehydrated, embedded in paraffin and sectioned at 5 µm thickness by the Elvie L. Taylor Histology Core Facility of Washington University. Antigen retrieval was performed in sodium citrate buffer (10 mM Tris–sodium citrate dihydrate pH 6.0, 0.05% Tween 20) followed by blocking of endogenous peroxidase activity in 3% hydrogen peroxide in TBS-T (0.1 M Tris–HCl pH 7.5, 0.15 M NaCl, 0.05% Tween 20). After blocking with 10% normal goat serum in TBS-T, samples were incubated overnight at 4 °C with rabbit anti–mouse Slc12a8 (1:100; ARP44039; Aviva) and subsequently with HRP-conjugated goat anti–rabbit immunoglobulin G (1:1,000) using the FITC TSA kit (Parkin Elmer) according to the manufacturer's protocol. Nuclei were stained with DAPI (Sigma-Aldrich). Digital images were collected with a fluorescence microscope (ApoTome 2; Zeiss).

Statistical analyses. Differences between two groups were assessed using the unpaired, two-tailed Student's *t*-test. Comparisons among several groups were performed using one-way ANOVA with various post hoc tests indicated in figure legends. *Z* ratios and two-sided *P* values for *Slc12a8* in Fig. 1a were calculated as previously described[48]. For comparisons, *P* values < 0.05 were considered statistically significant. All experiments were performed independently at least twice. GraphPad Prism (v.7) was used to conduct statistical analyses.

Reporting Summary. Further information on research design is available in the Nature Research Reporting Summary linked to this article.

Data availability

The microarray data used in this study has been deposited into the National Center for Biotechnology Information Gene Expression Omnibus (GEO) database (GEO accession numbers GSE49784 and GSE118365). All data generated or analysed during this study are included in the article and its Supplementary Information.

Received: 2 August 2018; Accepted: 29 October 2018;
Published online: 7 January 2019

References

1. Canto, C., Menzies, K. J. & Auwerx, J. NAD$^+$ metabolism and the control of energy homeostasis: a balancing act between mitochondria and the nucleus. *Cell Metab.* **22**, 31–53 (2015).
2. Rajman, L., Chwalek, K. & Sinclair, D. A. Therapeutic potential of NAD-boosting molecules: the in vivo evidence. *Cell Metab.* **27**, 529–547 (2018).
3. Verdin, E. NAD$^+$ in aging, metabolism, and neurodegeneration. *Science* **350**, 1208–1213 (2015).
4. Yoshino, J., Baur, J. A. & Imai, S. I. NAD$^+$ intermediates: the biology and therapeutic potential of NMN and NR. *Cell Metab.* **27**, 513–528 (2018).
5. Yoshino, J., Mills, K. F., Yoon, M. J. & Imai, S. Nicotinamide mononucleotide, a key NAD$^+$ intermediate, treats the pathophysiology of diet- and age-induced diabetes in mice. *Cell Metab.* **14**, 528–536 (2011).
6. Mouchiroud, L. et al. The NAD$^+$/sirtuin pathway modulates longevity through activation of mitochondrial UPR and FOXO signaling. *Cell* **154**, 430–441 (2013).
7. Camacho-Pereira, J. et al. CD38 dictates age-related NAD decline and mitochondrial dysfunction through an SIRT3-dependent mechanism. *Cell Metab.* **23**, 1127–1139 (2016).
8. Garten, A. et al. Physiological and pathophysiological roles of NAMPT and NAD metabolism. *Nat. Rev. Endocrinol.* **11**, 535–546 (2015).
9. Imai, S. Nicotinamide phosphoribosyltransferase (Nampt): a link between NAD biology, metabolism, and diseases. *Curr. Pharm. Des.* **15**, 20–28 (2009).
10. Belenky, P. et al. Nicotinamide riboside promotes Sir2 silencing and extends lifespan via Nrk and Urh1/Pnp1/Meu1 pathways to NAD$^+$. *Cell* **129**, 473–484 (2007).
11. Caton, P. W., Kieswich, J., Yaqoob, M. M., Holness, M. J. & Sugden, M. C. Nicotinamide mononucleotide protects against pro-inflammatory cytokine-mediated impairment of mouse islet function. *Diabetologia* **54**, 3083–3092 (2011).
12. de Picciotto, N. E. et al. Nicotinamide mononucleotide supplementation reverses vascular dysfunction and oxidative stress with aging in mice. *Aging Cell* **15**, 522–530 (2016).
13. Gomes, A. P. et al. Declining NAD$^+$ induces a pseudohypoxic state disrupting nuclear-mitochondrial communication during aging. *Cell* **155**, 1624–1638 (2013).
14. Long, A. N. et al. Effect of nicotinamide mononucleotide on brain mitochondrial respiratory deficits in an Alzheimer's disease-relevant murine model. *BMC Neurology* **15**, 19 (2015).

15. Mills, K. F. et al. Long-term administration of nicotinamide mononucleotide mitigates age-associated physiological decline in mice. *Cell Metab.* **24**, 795–806 (2016).
16. Stein, L. R. & Imai, S. Specific ablation of Nampt in adult neural stem cells recapitulates their functional defects during aging. *EMBO J.* **33**, 1321–1340 (2014).
17. Wang, X., Hu, X., Yang, Y., Takata, T. & Sakurai, T. Nicotinamide mononucleotide protects against β-amyloid oligomer-induced cognitive impairment and neuronal death. *Brain Res.* **1643**, 1–9 (2016).
18. Yamamoto, T. et al. Nicotinamide mononucleotide, an intermediate of NAD^+ synthesis, protects the heart from ischemia and reperfusion. *PLoS ONE* **9**, e98972 (2014).
19. Ramsey, K. M., Mills, K. F., Satoh, A. & Imai, S. Age-associated loss of Sirt1-mediated enhancement of glucose-stimulated insulin secretion in β cell-specific Sirt1-overexpressing (BESTO) mice. *Aging Cell* **7**, 78–88 (2008).
20. Revollo, J. R. et al. Nampt/PBEF/visfatin regulates insulin secretion in β cells as a systemic NAD biosynthetic enzyme. *Cell Metab.* **6**, 363–375 (2007).
21. Ratajczak, J. et al. NRK1 controls nicotinamide mononucleotide and nicotinamide riboside metabolism in mammalian cells. *Nat. Commun.* **7**, 13103 (2016).
22. Airhart, S. E. et al. An open-label, non-randomized study of the pharmacokinetics of the nutritional supplement nicotinamide riboside (NR) and its effects on blood NAD^+ levels in healthy volunteers. *PLoS ONE* **12**, e0186459 (2017).
23. Liu, L. et al. Quantitative analysis of NAD synthesis-breakdown fluxes. *Cell Metab.* **27**, 1067–1080 (2018).
24. Hebert, S. C., Mount, D. B. & Gamba, G. Molecular physiology of cation-coupled Cl^- cotransport: the SLC12 family. *Pflug. Arch.* **447**, 580–593 (2004).
25. Ramsey, K. M. et al. Circadian clock feedback cycle through NAMPT-mediated NAD^+ biosynthesis. *Science* **324**, 651–654 (2009).
26. Yamada, K., Hara, N., Shibata, T., Osago, H. & Tsuchiya, M. The simultaneous measurement of nicotinamide adenine dinucleotide and related compounds by liquid chromatography/electrospray ionization tandem mass spectrometry. *Anal. Biochem.* **352**, 282–285 (2006).
27. Shi, W. et al. Effects of a wide range of dietary nicotinamide riboside (NR) concentrations on metabolic flexibility and white adipose tissue (WAT) of mice fed a mildly obesogenic diet. *Mol. Nutr. Food Res.* 61, 1600878 (2017). .
28. Sociali, G. et al. Antitumor effect of combined NAMPT and CD73 inhibition in an ovarian cancer model. *Oncotarget* **7**, 2968–2984 (2016).
29. Alessi, D. R. et al. The WNK-SPAK/OSR1 pathway: master regulator of cation-chloride cotransporters. *Sci. Signal.* **7**, re3 (2014).
30. Belenky, P., Bogan, K. L. & Brenner, C. NAD^+ metabolism in health and disease. *Trends Biochem. Sci.* **32**, 12–19 (2007).
31. Bieganowski, P. & Brenner, C. Discoveries of nicotinamide riboside as a nutrient and conserved NRK genes establish a Preiss-Handler independent route to NAD^+ in fungi and humans. *Cell* **117**, 495–502 (2004).
32. Ummarino, S. et al. Simultaneous quantitation of nicotinamide riboside, nicotinamide mononucleotide and nicotinamide adenine dinucleotide in milk by a novel enzyme-coupled assay. *Food Chem.* **221**, 161–168 (2017).
33. Hewett, D. et al. Identification of a psoriasis susceptibility candidate gene by linkage disequilibrium mapping with a localized single nucleotide polymorphism map. *Genomics* **79**, 305–314 (2002).
34. Feigin, M. E. et al. Recurrent noncoding regulatory mutations in pancreatic ductal adenocarcinoma. *Nat. Genet.* **49**, 825–833 (2017).
35. Kim, J. E. et al. Associations between genetic polymorphisms of membrane transporter genes and prognosis after chemotherapy: meta-analysis and finding from Seoul Breast Cancer Study (SEBCS). *Pharmacogenomics J.* **18**, 633–645 (2018).
36. Wang, H. H., Patel, S. B., Carey, M. C. & Wang, D. Q. Quantifying anomalous intestinal sterol uptake, lymphatic transport, and biliary secretion in *Abcg8*$^{-/-}$ mice. *Hepatology* **45**, 998–1006 (2007).
37. Yoshino, J. & Imai, S. Accurate measurement of nicotinamide adenine dinucleotide (NAD^+) with high-performance liquid chromatography. *Methods Mol. Biol.* **1077**, 203–215 (2013).
38. Grimm, A. A., Brace, C. S., Wang, T., Stormo, G. D. & Imai, S. A nutrient-sensitive interaction between Sirt1 and HNF-1α regulates Crp expression. *Aging Cell* **10**, 305–317 (2011).
39. Revollo, J. R., Grimm, A. A. & Imai, S. The NAD biosynthesis pathway mediated by nicotinamide phosphoribosyltransferase regulates Sir2 activity in mammalian cells. *J. Biol. Chem.* **279**, 50754–50763 (2004).
40. Bruzzone, S. et al. The plant hormone abscisic acid increases in human plasma after hyperglycemia and stimulates glucose consumption by adipocytes and myoblasts. *FASEB J.* **26**, 1251–1260 (2012).
41. Bruzzone, S., Guida, L., Zocchi, E., Franco, L. & De Flora, A. Connexin 43 hemi channels mediate $Ca2^+$-regulated transmembrane NAD^+ fluxes in intact cells. *FASEB J.* **15**, 10–12 (2001).
42. Franco, L. et al. The transmembrane glycoprotein CD38 is a catalytically active transporter responsible for generation and influx of the second messenger cyclic ADP-ribose across membranes. *FASEB J.* **12**, 1507–1520 (1998).
43. Satoh, A. et al. Sirt1 extends life span and delays aging in mice through the regulation of Nk2 homeobox 1 in the DMH and LH. *Cell Metab.* **18**, 416–430 (2013).
44. Sato, T. & Clevers, H. Primary mouse small intestinal epithelial cell cultures. *Methods Mol. Biol.* **945**, 319–328 (2013).
45. Kolodziejska-Huben, M., Kaminski, Z. & Paneth, P. Preparation of ^{18}O-labelled nicotinamide. *J. Label. Compd. Radiopharm.* **45**, 1005–1010 (2002).
46. Chatterjee, A., Hazra, A. B., Abdelwahed, S., Hilmey, D. G. & Begley, T. P. A "radical dance" in thiamin biosynthesis: mechanistic analysis of the bacterial hydroxymethylpyrimidine phosphate synthase. *Angew. Chem. Int. Ed. Engl.* **49**, 8653–8656 (2010).
47. Fouquerel, E. et al. ARTD1/PARP1 negatively regulates glycolysis by inhibiting hexokinase 1 independent of NAD^+ depletion. *Cell Rep.* **8**, 1819–1831 (2014).
48. Cheadle, C., Vawter, M. P., Freed, W. J. & Becker, K. G. Analysis of microarray data using *Z* score transformation. *J. Mol. Diagn.* **5**, 73–81 (2003).

Acknowledgements

We thank C. Cantoni for flow cytometric analysis, L. Guida for support in proteoliposome preparation and R. Lewis for the production of *Slc12a8*-KO mice. We also thank E. Schulak for his generous support to A.G., members of the S.I. lab for critical comments and suggestions on this study and staff members in the core facilities provided by the Diabetes Research Center (P30 DK020579), the Nutrition Obesity Research Center (P30 DK56341) and the Hope Center for Neurological Disorders at Washington University. This work was also performed in a facility supported by NCRR grant C06 RR015502. A.G. was supported as the Tanaka Scholar by T. Tanaka and M. Tanaka. M.E.M was supported by UK Research Councils and Biotechnology and Biological Science Research Council (BBSRC; BB/N001842/1). This work was mainly supported by grants from the National Institute on Aging (AG024150, AG037457, AG047902) to S.I.

Author contributions

S.I. conceived the project, and A.G. and S.I. mainly designed research, analysed data and wrote the manuscript. A.G. performed most experiments. K.F.M. performed the analyses of gut-specific *Slc12a8*-KD mice and whole-body *Slc12a8*-KO mice with A.G. J.Y. performed microarray analyses. S.B. and G.S. conducted proteoliposome experiments and analysed the results with A.G. and S.I. K.T. and A.G. performed immunostaining, and H.C.L. and A.G. conducted *Slc12a8* overexpression in vivo. R.C. and M.E.M. synthesized O18-D-NR and O18-D-NMN for this study, and Y.S. and A.G. conducted mass spectrometry analyses.

Competing interests

A.G. and S.I. are inventors on a patent (PCT/US18/46233) about the Slc12a8 NMN transporter, whose applicant is Washington University and which has been licensed by Teijin Limited (Japan). Other authors declare no competing interests.

Additional information

Supplementary information is available for this paper at https://doi.org/10.1038/s42255-018-0009-4.

Reprints and permissions information is available at www.nature.com/reprints.

Correspondence and requests for materials should be addressed to S.I.

Publisher's note: Springer Nature remains neutral with regard to jurisdictional claims in published maps and institutional affiliations.

nature research

Corresponding author(s): DBPR, NATMETAB-A18080316B

Reporting Summary

Nature Research wishes to improve the reproducibility of the work that we publish. This form provides structure for consistency and transparency in reporting. For further information on Nature Research policies, see Authors & Referees and the Editorial Policy Checklist.

Statistical parameters

When statistical analyses are reported, confirm that the following items are present in the relevant location (e.g. figure legend, table legend, main text, or Methods section).

n/a	Confirmed	
☐	☒	The exact sample size (*n*) for each experimental group/condition, given as a discrete number and unit of measurement
☐	☒	An indication of whether measurements were taken from distinct samples or whether the same sample was measured repeatedly
☐	☒	The statistical test(s) used AND whether they are one- or two-sided *Only common tests should be described solely by name; describe more complex techniques in the Methods section.*
☒	☐	A description of all covariates tested
☐	☒	A description of any assumptions or corrections, such as tests of normality and adjustment for multiple comparisons
☐	☒	A full description of the statistics including central tendency (e.g. means) or other basic estimates (e.g. regression coefficient) AND variation (e.g. standard deviation) or associated estimates of uncertainty (e.g. confidence intervals)
☐	☒	For null hypothesis testing, the test statistic (e.g. *F*, *t*, *r*) with confidence intervals, effect sizes, degrees of freedom and *P* value noted *Give P values as exact values whenever suitable.*
☒	☐	For Bayesian analysis, information on the choice of priors and Markov chain Monte Carlo settings
☒	☐	For hierarchical and complex designs, identification of the appropriate level for tests and full reporting of outcomes
☒	☐	Estimates of effect sizes (e.g. Cohen's *d*, Pearson's *r*), indicating how they were calculated
☐	☒	Clearly defined error bars *State explicitly what error bars represent (e.g. SD, SE, CI)*

Our web collection on statistics for biologists may be useful.

Software and code

Policy information about availability of computer code

Data collection	no software was used
Data analysis	GraphPad 7 (Prism) for Mac OS Kaluza 1.3 (Beckman coulter) Adobe Photoshop CC 2015 Clustal Omega(EMBL-EBI) TMHMM Server v. 2.0 (Expasy) MassHunter(Agilent)

For manuscripts utilizing custom algorithms or software that are central to the research but not yet described in published literature, software must be made available to editors/reviewers upon request. We strongly encourage code deposition in a community repository (e.g. GitHub). See the Nature Research guidelines for submitting code & software for further information.

Data

Policy information about availability of data

All manuscripts must include a data availability statement. This statement should provide the following information, where applicable:

- Accession codes, unique identifiers, or web links for publicly available datasets
- A list of figures that have associated raw data
- A description of any restrictions on data availability

The microarray data used in this study has been deposited into the NCBI GEO database (GEO accession numbers GSE49784 and GSE118365). The data set will be released to the public before publication of this paper. All data generated or analyzed during this study are included in the article and its Supplementary Information.

Field-specific reporting

Please select the best fit for your research. If you are not sure, read the appropriate sections before making your selection.

☒ Life sciences ☐ Behavioural & social sciences ☐ Ecological, evolutionary & environmental sciences

For a reference copy of the document with all sections, see nature.com/authors/policies/ReportingSummary-flat.pdf

Life sciences study design

All studies must disclose on these points even when the disclosure is negative.

Sample size	No statistical calculation was performed to predetermine sample size because it is difficult to estimate the extent of biological variation in each case. Nonetheless, for cell culture experiments, we usually have duplicates or triplicates per experiment and repeat the experiment three to four times, which usually provides statistically significant differences. For animal experiments, we usually require 15-20 mice for each sex of experimental and control mice to distinguish a difference of 10-15% in metabolic parameters with power >= 0.80 and p <= 0.05 in the two-tailed t test. In this study, the differences were larger so that the numbers of mice we used were less than this estimation.
Data exclusions	If experimental procedures or measurements fail so that accurate data cannot be obtained for certain samples, these particular data sets would be excluded from the final data analyses. Reasons for which included suboptimal lentivirus knockdown efficiency and poor resolution of HPLC' s chromatogram.
Replication	For primary cell cultures, replicates of cells from the same animal are considered to be technical replicates. Therefore, we usually use three to four animals (biological replicates) and make at least two-three technical replicates per animal. For established cell lines, independent experimental procedures or treatments are considered to be biological/technical replicates. We usually have duplicates or triplicates per experiment and repeat the experiment three to four times, which provides 6-12 independent data points. For animal experiments, we use at least two to three different cohorts (different litters). Each cohort include at least 3-4 mice each for sex and genotype. Replicate experiments were successful.
Randomization	For cell culture experiments, no randomization is usually performed. For animal experiments, each cohort is usually chosen randomly, and experimental procedures are applied to animals in a random order.
Blinding	Investigators were not blinded to group allocation during data collection and analysis. Data reported for mouse experiments and cell cultures experiment are not subjective but rather based on quantitative High Performance Liquid Chromatography (HPLC) and Mass Spectrometry, flow cytometry, and scintillation counter detection.

Reporting for specific materials, systems and methods

Materials & experimental systems

n/a	Involved in the study
☐	☒ Unique biological materials
☐	☒ Antibodies
☐	☒ Eukaryotic cell lines
☒	☐ Palaeontology
☐	☒ Animals and other organisms
☒	☐ Human research participants

Methods

n/a	Involved in the study
☒	☐ ChIP-seq
☐	☒ Flow cytometry
☒	☐ MRI-based neuroimaging

Unique biological materials

Policy information about availability of materials

Obtaining unique materials	All unique materials are readily available from the authors for distribution to academic scientists. For for-profit companies and institutes, the Material Transfer Agreement will need to be processed between Washington University and these companies/ institutes.

Antibodies

Antibodies used	We used: The polyclonal rabbit anti-mouse Slc12a8 (catalog #ARP44039, Aviva, CA), polyclonal rabbit anti-mouse Caveolin-1 (catalog #3238, Cell Signaling, MA), monoclonal anti-GAPDH (catalog # MAB374, Millipore, CA,), anti-FLAG MS (1:500, #F3165, Sigma, MO). Polyclonal rabbit antiserum was produced against a synthetized N-terminal peptide (AQRSPQELFHEAAQQGC) of mouse Slc12a8 by Covance. Polyclonal goat anti-rabbit IgG (H+L) conjugated with Alexa Flour 488 (catalog#A-11034, Invitrogen) and Zombie Dye (catalog #423101 , Biolegend).
Validation	The polyclonal rabbit anti-mouse Slc12a8 (catalog #ARP44039, Aviva, CA), polyclonal rabbit anti-mouse Caveolin-1 (catalog #3238, Cell Signaling, MA), monoclonal anti-GAPDH (catalog # MAB374, Millipore, CA,), anti-FLAG MS (1:500, #F3165, Sigma, MO) were validated by manufacturer for Western blot analysis on murine cell lines. Polyclonal rabbit antiserum was produced against a synthetized N-terminal peptide (AQRSPQELFHEAAQQGC) of mouse Slc12a8 by Covance. We have validated Covance's Slc12a8 antisera by performing Western blot analysis on mouse tissues from Slc12a8KO mice and their wild-type littermates. Polyclonal goat anti-rabbit IgG (H+L) conjugated with Alexa Flour 488 (catalog#A-11034, Invitrogen) and Zombie Dye (catalog #423101 , Biolegend) were validated by manufacture for Flow Cytometry analysis.

Eukaryotic cell lines

Policy information about cell lines

Cell line source(s)	NIH3T3 cell line was originally purchased from the American Type Culture Collection (ATCC).
Authentication	None of the cell lines used have been authenticated
Mycoplasma contamination	The NIH3T3 cell line we used in this study was tested and found negative for micoplasma contamination.
Commonly misidentified lines (See ICLAC register)	No commonly misidentified cell lines were used.

Animals and other organisms

Policy information about studies involving animals; ARRIVE guidelines recommended for reporting animal research

Laboratory animals	We used : Female C57BL/6J mice (Provider:Jackson Laboratories) at 2-24 months of age, Male C57BL/6J mice (Provider:Jackson Laboratories) at 3-4 months of age, Female C57BL/6J mice (From NIA housed in Charles River facility) at 3-26 months of age and whole-body Slc12a8KO mice and their wild-type littermates (strain:C57BL/6J) at 2-10 months of age, generated and housed in our laboratory.
Wild animals	This study did not involve wild animals
Field-collected samples	This study did not involve samples collected from the field.

Flow Cytometry

Plots

Confirm that:

☐ The axis labels state the marker and fluorochrome used (e.g. CD4-FITC).

☐ The axis scales are clearly visible. Include numbers along axes only for bottom left plot of group (a 'group' is an analysis of identical markers).

☐ All plots are contour plots with outliers or pseudocolor plots.

☒ A numerical value for number of cells or percentage (with statistics) is provided.

Methodology

Sample preparation	NIH3T3 cells were incubated with DMSO 0.1%, FK866 100 nM or FK866 100 nM and NMN 100 uM for 48h at 37C. Cells were

Sample preparation	then washed once with cold PBS, treated with 0.02%EDTA in PBS and stained for flow cytometry using a polyclonal rabbit anti-mouse Slc12a8 antibody(ARP44039) at 1:200, a secondary goat anti-rabbit IgG conjugated with Alexa Fluor 488 at 1:2000 and the survival market Zombie Dye at 1:400 for 25 min at 4C. For the intracellular staining, cells were fixed in 2% PFA for 10 min at RT and then permeabilized in saponin-conteining buffer for 10 min at RT. Slc12a8 staining was performed in permeabilization buffer for 25 min at 4C. 1x 106 cells for each condition were used for flow cytometry analysis.
Instrument	Gallios Flow cytometer 10 color/3 laser from Beckman Coulter (serial number AU25604)
Software	Kaluza 1.3
Cell population abundance	We used NIH3T3 cell line so only one type of cell. The purity of the samples was not determined
Gating strategy	NIH3T3 cells were a unique and homogeneous population on FSC/SSC gates. NIH3T3 cells stained with only secondary antibody conjugated with Alexa Flour 488 were used as negative control. Positive cells for Slc12a8/Alexa Flour 488 staining were selected, based on Zombie Dye/SSC negative cells.

☐ Tick this box to confirm that a figure exemplifying the gating strategy is provided in the Supplementary Information.